Cellulose (2022) 29:6579–6593
https://doi.org/10.1007/s10570-022-04669-5

ORIGINAL RESEARCH

Structure–activity relationship of thermal interaction between arylmalonamide[70]fullerocyclopropane stabilizer and nitrocellulose

Yang Zhao · Bo Jin · Tian Zheng · Rufang Peng

Received: 2 March 2022 / Accepted: 13 May 2022 / Published online: 21 June 2022

Abstract The thermal decomposition or even explosion of nitrocellulose during long-term storage is prevented by adding stabilizers to nitrocellulose-based propellants. A series of novel arylmalonamide[70]fullerocyclopropane (**3a–c**) were synthesized through Bingel reaction. The molecular structures of **3a–c** were verified through ^{1}H NMR, ^{13}C NMR, Fourier transform infrared spectroscopy (FT-IR), UV–visible spectroscopy, and mass spectrum. The thermal stability of **3a–c** to nitrocellulose was studied by methyl violet paper test and iso-thermogravimetry method, and the results showed that the stability of **3a–c** to nitrocellulose was significantly better than that of the [60]fullerene-based stabilizers. The thermal stability of **3a–c** to nitrocellulose improved as the increase of the carbon chain length on the *p*-position of the benzene ring. The effects of **3a–c** on the thermal decomposition of nitrocellulose were obtained by differential thermal analysis, and the results showed that the critical temperature of the thermal explosion of nitrocellulose can be increased by 0.1–2.8 °C by **3a–c**. The thermal stability of **3a–c** to nitrocellulose in adiabatic environment was confirmed by accelerating rate calorimetry. In addition, the stabilization mechanism was studied through ESR and FT-IR, and the results showed that **3a–c** can react with nitrogen oxide radicals released by nitrocellulose. These arylmalonamide[70]fullerocyclopropane with excellent thermal stability and strong radical scavenging ability can be used as a promising stabilizer for single and double based propellants.

Keywords Fullerocyclopropane · Stabilizer · Nitrocellulose · Arylmalonamide · Thermal decomposition

Introduction

High nitrogen content nitrocellulose, which is a kind of flammable polymer has energy characteristics and can provide power for propellant combustion (Tarchoun et al. 2021, 2022a, b, 2022c). Nitrocellulose-based propellants are widely used in missile launchers to provide energy for rocket systems (Srinivas et al. 2016; Agrawal et al. 2000). However, owing to the special chemical structure of nitrate, an O–NO_2 bond with weak bond energy is prone to mild thermal decomposition in long-term storage and transportation (Luo et al. 2019; Trache et al. 2019; Wang et al. 2017). The decomposition products of

Supplementary Information The online version contains supplementary material available at https://doi.org/10.1007/s10570-022-04669-5.

Y. Zhao · B. Jin (✉) · T. Zheng · R. Peng (✉)
State Key Laboratory of Environment-Friendly Energy Materials, Southwest University of Science and Technology, Mianyang 621010, Sichuan, China
e-mail: jinbo0428@163.com

R. Peng
e-mail: rfpeng2006@163.com

propellant further accelerate the thermal decomposition of nitrate and eventually induce propellant to emit large amounts of heat that lead to performance failure and even cause combustion explosion accidents (Sun et al. 2017; Shehata et al. 2003; Naud et al. 1992). Some traditional chemical stabilizers, mainly aniline and phenylurea compounds, are added to propellants to inhibit the autocatalytic reactions of nitrate esters and extend the service lives of propellants (Trache et al. 2013; Drzyzga et al. 2003; Tong et al. 2001). In addition, some novel biological macromolecules stabilizers have been studied by many researches but they are not received any industrial applications like traditional aromatic amine stabilizers (Cherif et al. 2020a, b, 2021). However, the most common traditional aromatic amine stabilizers have poor thermal stability, high toxicity, and poor stability effect under extreme conditions (De Klerk et al. 2015; Fryš et al. 2011; Lussier et al. 2006; Lindblom et al. 2002). The autocatalytic decomposition of nitrate can be inhibited by traditional aromatic amines stabilizers given that the alkaline compounds of aromatic amines can quickly combine with nitrogen oxides, but their strong alkalinity promotes the saponification of nitrate and reduces the chemical stability of the propellant, greatly limiting the application of weapon systems (Katoh et al. 2007). In addition, the stability of traditional stabilizers decreases at high temperature. The traditional stabilizer cannot meet the requirements and development of modern weapons. Therefore, the development of novel stabilizers are urgently essential.

Electron-withdrawing carbonyl group was introduced into the amino group inn the aromatic amine to form phenylurea derivative, reducing its basicity and the possibility of saponification. However, as a weakly basic compound, although the phenylurea derivatives also have the ability to absorb nitrogen oxides, their thermal stability to nitrocellulose is weak (Tang et al. 2017; Krumlinde et al. 2016). Bergmann and Junk test showed that the malonamide derivatives could effectively improve the thermal stability of nitrocellulose, and the stability effect was stronger than the traditional stabilizer C1. The charge effect of the substituent group affected the thermal stability of the malonamide derivatives (Zayed et al. 2010; Hassan et al. 2001; Zayed et al. 2000). Moreover, fullerene has the advantages of good thermal stability, strong acid resistance, and oxidation resistance owing to its good radical scavenging ability of various radicals, and has good compatibility with the main components of propellants (Dogru et al. 2012; Krishna et al. 2010; Dennler et al. 2009; Markovic et al. 2008; Jia et al. 2005; Butts et al. 2003). Therefore, fullerene-phenylurea derivatives are considered potential fullerene-based stabilizers (Li et al. 2020). Compared with other fullerene-based stabilizers, fullerocyclopropane derivatives have some advantages, such as weak alkalinity, high yield and no large amounts of by-products (Liao et al. 2021; Zhao et al. 2020a, b; Chai et al. 2020). The effect of C_{70}-phenylurea derivatives, which have stronger electron absorption and π electron conjugation effects than that of C_{60}-phenylurea derivatives on the thermal stability of nitrocellulose, have not been studied (Dresselhaus et al. 1996; Xie et al. 1992).

A series of C_{70} derivatives, arylmalonamide[70] fullerocyclopropane, were successfully synthesized using the Bingel reaction for the first time. The thermal stability of arylmalonamide[70]fullerocyclopropane on nitrocellulose was determined with isothermal experiments, and the stabilization mechanism and thermal behavior of arylmalonamide[70]fullerocyclopropane in the thermal decomposition of nitrocellulose were examined through non-isothermal thermal analysis. The thermal stability of arylmalonamide[70] fullerocyclopropane with different functional groups to nitrocellulose was evaluated.

Experimental sections

Synthesis procedures

All the reagents for organic synthesis were purchased from Aladdin Industrial Corporation, and organic solvents were purchased from Kelong Chemical Reagents Corporation. Fullerene C_{70} was obtained from Puyang Yongxin Fullerene Technology Corporation.

Synthesis of *p*-aryl malonamide derivatives: 4 mmol *p*-methylaniline (**1a**, 428 mg) or *p*-methoxyaniline (**1b**, 492 mg) or *p*-ethoxyaniline (**1c**, 548 mg) was dissolved in 40 mL of resteamed dichloromethane, and triethylamine (1 mL, 4 mmol) was added as the acid-binding agent. In an ice bath, the dichloromethane diluent (0.08 M) of malonyl chloride was added slowly using a constant pressure drop funnel, and the mixture was stirred for 0.5 h. Then, the

reaction was continued at room temperature for 6 h. After the reaction, the solution was washed several times with distilled water, and the excess dichloromethane solvent was removed. The obtained light yellow solid products were recrystallized with ethyl acetate, and white solid malonamide derivatives (**2a–c**) were obtained through vacuum desiccation in yields of 86, 88 and 89%, respectively. The characterization results were shown in Figs. S1 – 9. *p*-toluene malonamide (**2a**): ^{1}H NMR (600 MHz, d-DMSO) δ/ppm 10.10(s, 2H); 7.49(d, 4H, J = 8.41), 7.11(d, 4H, J = 8.27), 3.44(s, 2H), 2.25(s, 6H); ^{13}C NMR (150 MHz, d-DMSO) δ/ppm 165.68, 136.96, 132.72, 129.58, 119.53, 56.31, 20.91; FTIR ν/cm^{-1} (KBr) 3136 (Ar–H), 2924 (–CH_3), 1741 (C = O), 1650, 1531, 1407 (Ar), 1250 (Ar–N–), 818 (C–H). *p*-methoxyphenyl malonamide (**2b**): ^{1}H NMR (600 MHz, d-DMSO) δ/ppm 10.03(s, 2H), 7.52(d, 4H, J = 9.01), 6.89(d, 4H, J = 9.06), 3.72(s, 6H), 3.41(s, 2H); ^{13}C NMR (150 MHz, d-DMSO) δ/ppm 164.89, 155.15, 132.05, 120.49, 113.75, 55.04, 45.51; FTIR ν/cm^{-1} (KBr) 3053 (Ar–H), 2929 (–CH_3), 1740 (C = O), 1642, 1549, 1512, 1411 (Ar), 1244 (Ar–N–), 1032 (C–O–C), 823 (C–H). *p*-ethoxyphenyl malonamide (**2c**): ^{1}H NMR (600 MHz, d-DMSO) δ/ppm 10.30(s, 2H), 7.54(d, 4H, J = 9.01), 6.86(d, 4H, J = 9.04), 3.98(q, 4H, J = 6.96), 3.44(s, 2H), 1.30(t, 6H, J = 6.96); ^{13}C NMR (150 MHz, d-DMSO) δ/ppm 165.37, 154.91, 132.69, 120.94, 114.80, 63.52, 46.27, 15.16; FTIR ν/cm^{-1} (KBr) 3048 (Ar–H), 2976, 2943 (–CH_2–, –CH_3), 1646, 1549, 1513, 1396 (Ar), 1243 (Ar–N–), 1052 (C–O–C), 823 (C–H).

Synthesis of arylmalonamide[70]fullerocyclopropane: arylmalonamide[70]fullerocyclopropane were synthesized using the Prato reaction. C_{70} (84 mg, 0.1 mmol), malonamide derivatives (**2a/2b/2c**, 28 mg/32 mg/34 mg, 0.1 mmol), DBU (23 μL, 0.15 mmol), and CBr_4 (50 mg, 0.15 mmol) were completely dissolved in 50 mL of toluene. The reaction was stirred at 5 ℃ under nitrogen protection for 0.5 h. After the reaction, impurities were removed through filtration, and the solvent was removed through rotary evaporation. The crude products were separated and purified through silica gel column chromatography. First, unreacted C_{70} was eluted with CS_2, and then dichloromethane/tetrahydrofuran was used as the eluent. Dark brown solid arylmalonamide[70]fullerocyclopropanes (**3a–c**) were obtained in yields of 30%, 36% and 34%. The process is shown in Fig. 1.

Characterization

^{1}H NMR and ^{13}C NMR spectra were obtained using a Bruker Avance 600 spectrometer. Residual $CHCl_3$ or DMSO was detected at 7.26 or 2.49 ppm in the ^{1}H NMR spectra, respectively. and residual $CHCl_3$ or DMSO was detected at 77.16 or 39.52 ppm in the ^{13}C NMR spectra, respectively. Fourier transform infrared (FT-IR) spectra were recorded with a Nicolet 380 FT-IR spectrophotometer using spectrograph KBr in a range of 4000 – 400 cm^{-1}. The UV–vis spectrophotometer with a double-beam light source of 190 – 1100 nm was used. The mass spectrum analysis was conducted using an Varian 1200 LC/MS.

Nitrocellulose samples preparation

Nitrocellulose with nitrogen content of 12.76% was supplied by the China Academy of Engineering Physics.

Nitrocellulose samples were prepared with the solvent evaporation method, and the preparation process

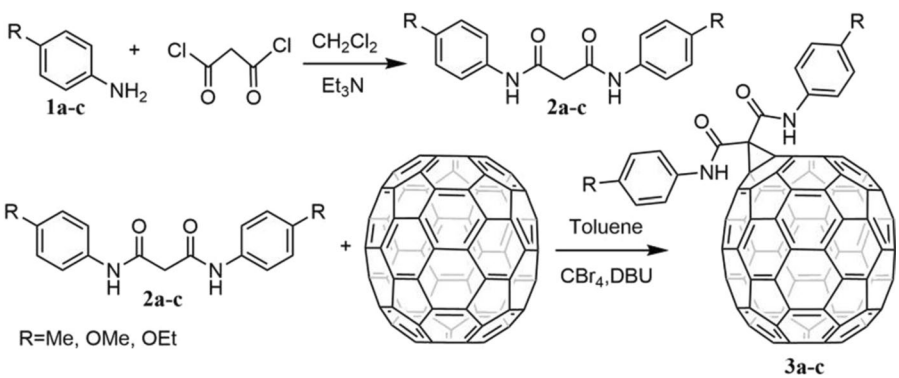

Fig. 1 Synthetic route of arylmalonamide[70]fullerocyclopropanes (R = **3a**: Me; **3b**: OMe; **3c**: OEt)

was showed in Fig. S10. First, stabilizers (9 mg) were dissolved in 1 mL of CS_2 to form a uniform solution. Then, 291 mg of nitrocellulose was added, and the solution was stirred for 1 h. The solvent was evaporated. The resulting uniform mixture was dried in a vacuum oven at 45 ℃ for 48 h. The composition of each nitrocellulose sample is listed in Table 1.

The compatibility between stabilizer and nitrocellulose was obtained by differential thermal analysis. The test results were shown in Table S1, which shows that the **3a–c** has good compatibility with nitrocellulose.

Thermal stability analysis

Methyl violet test was performed with the GJB 770B-2005 method. The nitrocellulose sample was heated in a test tube at 134.5 °C with a sample mass of 300 mg in the presence of methyl violet paper. Subsequently, time was measured until the color of the paper changes from purple to salmon pink. Differential thermal analysis (DTA) was performed using a WCR-1B differential thermal analyzer at a heating rate of 10 °C·min^{-1}. Thermogravimetric (TG) analysis was performed at constant temperatures of 135, 145 and 155 °C with a WRT-1D thermal analyzer. Differential scanning calorimetry (DSC) analysis was carried out with a Q200 (USA) TA instrument at a heating rate of 10 °C·min^{-1}. The "interruption and re-scanning" method described in previous studies was used (Wang et al. 2015). The accelerating rate calorimetry (ARC) was carried out on a NETZSCH instrument, and a titanium bomb with a thermocouple clip at the bottom was used. The heating–searching–waiting (H–W–S) mode procedure was carried out at a heating rate of 10 °C·min^{-1} and a searching time of 30 min, and the sample masses was 40.0 ± 0.1 mg.

Stability mechanism analysis

ESR spectrometry was performed using a Bruker EMXmicro instrument. The settings were as follows: microwave power, 2 mW; modulation frequency, 100 kHz; field center, 3440 G; sweep width, 100 G; conversion time, 40.04 ms; time constant, 40.96 s; number of scans, 3; and sweep time, 60.06 s.

Table 1 Composition of the nitrocellulose sample

Sample	S-1	S-2	S-3	S-4
Stabilizer (wt/%)	–	**3a** (3%)	**3b** (3%)	**3c** (3%)

Results and discussion

Structural characterization

The structures of arylmalonamide[70]fullerocyclopropanes (**3a–c**) were characterized through ^{1}H NMR, ^{13}C NMR, FT-IR, UV–vis, and LC–MS spectra. The ^{1}H NMR spectrum of **3c** is shown in Fig. 2(a). Two doublets at δ 7.42 and 6.83 ppm appeared in the hydrogen proton region of the benzene ring, and the hydrogen area integral ratio was 2:2. One quartet at δ 4.00 ppm and one triplet at δ 4.18 ppm were obtained in a hydrogen area integral ratio of 2:3, which were attributed to the methylene and methyl groups in ethoxy, respectively. One singlet appears at δ 9.00 ppm, which was attributed to amino proton. The ^{13}C NMR spectrum of **3c** (Fig. 2(b)) displayed signals at δ of 155.26 − 131.18 ppm for the carbon atoms on C_{70}. The signals at δ 122.09 − 114.73, 156.11, and 130.28 ppm were phenyl carbons connected to hydrogen, ethoxyl, and amino, respectively. The signals at δ 99.97 − 77.52 and 44.25 ppm were attributed to the methylene carbon on the cyclopropane and the sp^3 carbon of C_{70} connected with cyclopropane, respectively. The signals at δ 63.67 and 14.83 ppm were attributed to the ethoxyl carbon. The signal at δ 165.42 ppm was attributed to the carboxyl carbon. The structures of **3c** was a completely symmetric *p*-ethoxyphenyl malonamide[70]fullerocyclopropane. The results were consistent with the ^{1}H NMR and ^{13}C NMR spectra (Figs. S11–14) of 3a–b. Subsequently, LC–MS spectra results further indicated that 3a-c were monoaddition C_{70} derivatives (Figs. S15 − 17).

The structures of **3a–c** were confirmed using FT-IR spectra, as shown in Fig. 3. The stretching vibration absorption peak at 3430 cm^{-1} was attributed to the N − H bond. The absorption peaks at 2920 − 2845 cm^{-1} were attributed to C − H bond. The stretching vibration absorption peak at 1737 cm^{-1} was attributed to carbonyl C = O bond. The absorption peaks at 1640 − 1510 cm^{-1} were attributed to the benzene ring skeleton. The characteristic absorption peaks of C_{70} were detected at 1377 and 526 cm^{-1}. The characterization results were consistent with the target functional groups.

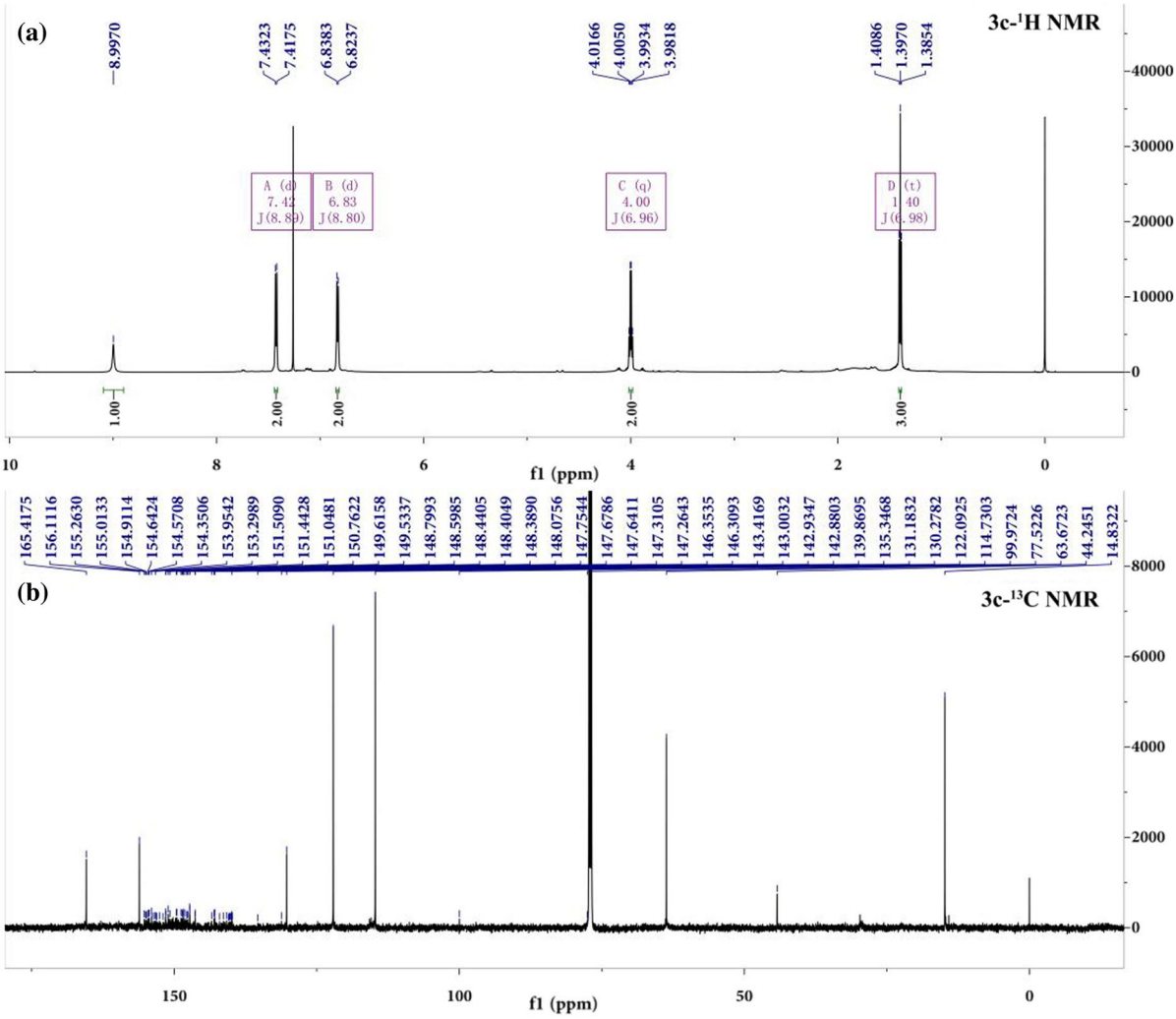

Fig. 2 ^{1}H NMR (**a**) and ^{13}C NMR (**b**) of **3c**

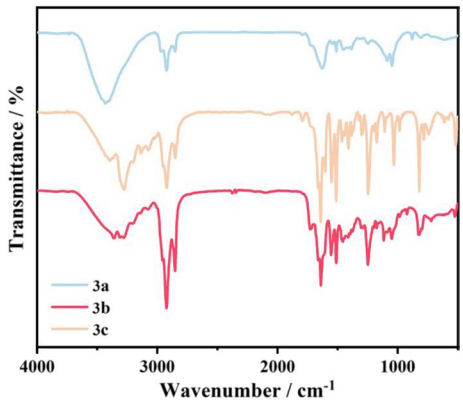

Fig. 3 FT-IR spectra of **3a–c**

The absorption peak at 441.5 nm in the UV–Vis spectra of **3a–c** (Fig. 4) was attributed to the C1 − C2 bond of C_{70} derivatives (Wang et al. 2010). It indicated that the structure of **3a–c** conformed to expectations.

Stability experiment

The thermal stability of nitrocellulose was evaluated through isothermal thermal analysis, and the thermal decomposition reactions of different nitrocellulose samples at a constant temperature were measured. The common methods included volumetric gas and gravimetric methods. First, the methyl purple paper

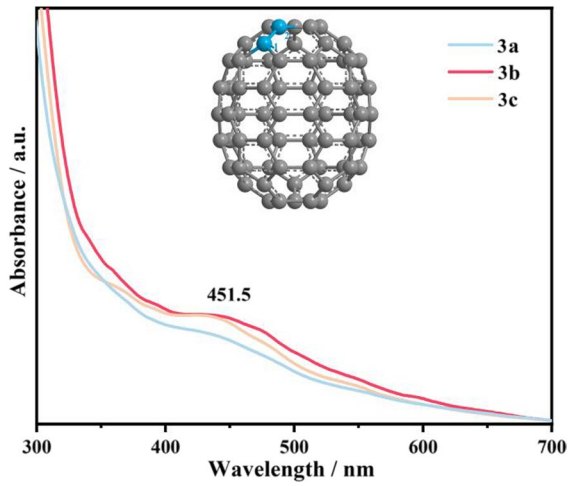

Fig. 4 UV – vis spectra of **3a–c**

Table 2 Discoloration time of the methyl violet paper test at 134.5 °C

Sample	S-1	S-2	S-3	S-4
Stabilizer	–	**3a**	**3b**	**3c**
Time/min	58	128	132	139
Storage for 5 h	Non-burning and non-exploding			

method was used to evaluate the stability of **3a–c** to nitrocellulose, and the temperature was 134.5 °C. The discoloration times of S-1–S-4 in the methyl purple paper test were shown in Table 2. **3a–c** extended the discoloration time of methyl purple paper test of nitrocellulose by 70, 74, and 81 min, respectively. Nitrocellulose samples S-1–S-4 did not burn or deignite after heating for 5 h, and the discoloration time of S-1–S-4 was longer than the previous results (Li et al. 2020), indicating that the stability of **3a–c** were superior to that of the previously reported arylmalonamide[60]fullerocyclopropane.

In the thermogravimetric method, weight loss of nitrocellulose samples at constant temperature was used as a standard for evaluating the thermal stability of nitrocellulose samples. Isothermal thermogravimetry was conducted at 135, 145 and 155 °C, which were all higher than the temperature for the methyl violet paper test. The results are shown in Fig. 5(a–c), the weight loss of nitrocellulose samples S-1–S-4 increased with temperature. Weight loss of the nitrocellulose samples S-2–S-4 after the addition of **3a–c** was obviously weaker than that of nitrocellulose S-1, indicating that **3a–c** can effectively alleviate the thermal decomposition of nitrocellulose. The order by degree of influence was consistent with that of the methyl violet paper test.

The safe storage life of nitrocellulose samples were obtained through isothermal kinetics at different temperatures. The weight loss of nitrocellulose was 1.6% when the methyl violet test paper changed color. Then, the time required when the weight loss of nitrocellulose samples reached 1.6% was taken as the evaluation standard. The time required for different nitrocellulose samples S-1–S-4 to reach 1.6% weight loss was shown in Table S2. The safe storage life can be calculated according to Semenov's equation:

$$\ln t_{\mathrm{T}} = \mathrm{a} + \frac{\mathrm{b}}{T} \tag{1}$$

where T is the constant temperature, K; t_{T} is the time required for the weight loss to reach 1.6% at temperature T, min; a and b are coefficients.

The fitting curves of Semenov's equation for the nitrocellulose samples S-1–S-4 were shown in Fig. 5(d), and the calculation results were shown in Table 3. The safe storage life of the nitrocellulose samples increased gradually from S-1 to S-4, indicating that **3a–c** can effectively prolong the safe storage life of nitrocellulose. The sequence of **3a–c** was consistent with that of the thermal stability of nitrocellulose samples S-1–S-4.

Thermal interaction test

The non-isothermal thermodynamics reflected the ability of **3a–c** to interact with nitrocellulose. The activation energy of thermal decomposition generally reflects the thermal decomposition capacities of samples, and the autocatalytic decomposition products released by nitrocellulose during thermal decomposition can catalyze the thermal decomposition of nitrocellulose. Therefore, the thermal decomposition activation energy of nitrocellulose can be affected theoretically after the heating process. The nitrocellulose samples S-1–S-4 before and after the methyl violet paper test were subjected to DTA tests at different heating rates (5, 10, 15 and 20 C min^{-1}). The DTA curves obtained were showed in Fig. 6 and Fig. S18.

According to the thermal decomposition temperature of nitrocellulose samples S-1–S-4, the thermal

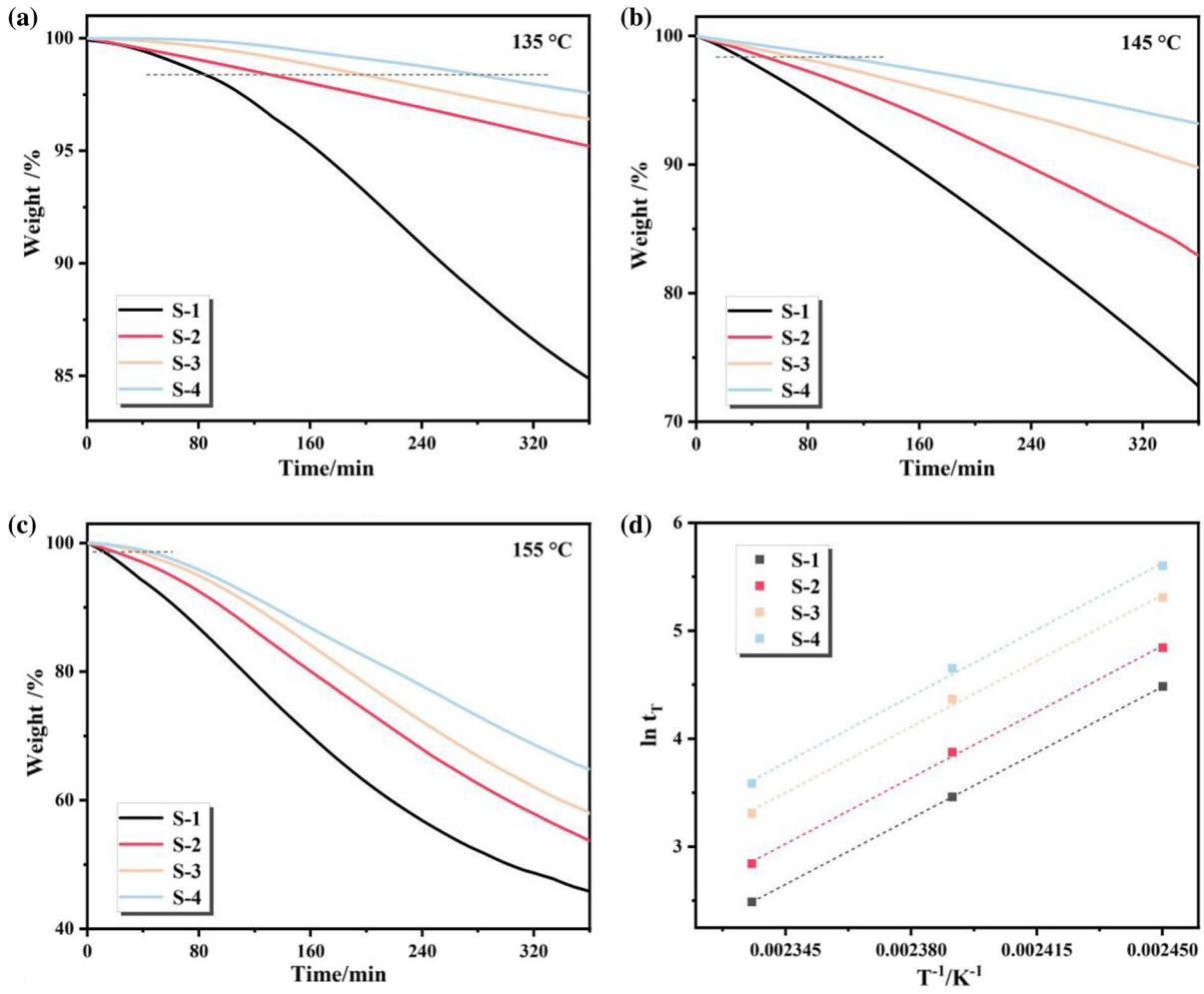

Fig. 5 Isothermal TG curves of nitrocellulose samples S-1–S-4 at 135 °C (**a**), 145 °C (**b**), 155 °C (**c**), and the fitting curves of Semenov's equation for the nitrocellulose samples S-1–S-4 (**d**)

Table 3 Empirical formula and storage life at different rates of weight loss in S-1–S-4

α	Empirical formula	R^2	Storage life (a)	
			25 °C	50 °C
S-1–1.6%	$\ln t_T = 17{,}433.82/T - 38.23$	0.9998	1177.35	12.77
S-2–1.6%	$\ln t_T = 17{,}466.66/T - 37.93$	0.9980	1774.31	19.09
S-3–1.6%	$\ln t_T = 17{,}441.35/T - 37.40$	0.9955	2769.10	29.98
S-4–1.6%	$\ln t_T = 17{,}609.22/T - 37.52$	0.9955	4312.69	44.71

decomposition parameters were calculated by using Kissinger equation Eqs. 2, 3, and 4.

$$\ln \frac{\beta}{T_p^2} = \ln \frac{AR}{E_a} - \frac{E_a}{RT_p} \tag{2}$$

$$T_{pi} = T_{p0} + b\beta_i + c\beta_i^2 + d\beta_i^3 \tag{3}$$

$$T_{bp0} = \frac{E_a - \sqrt{E_a^2 - 4E_aRT_{p0}}}{2R} \tag{4}$$

where β is the gas constant (8.314 $J \cdot mol^{-1} \cdot K^{-1}$); T_p is the peak temperature of the DTA curve; E_a is the value of the activation energy; A is the

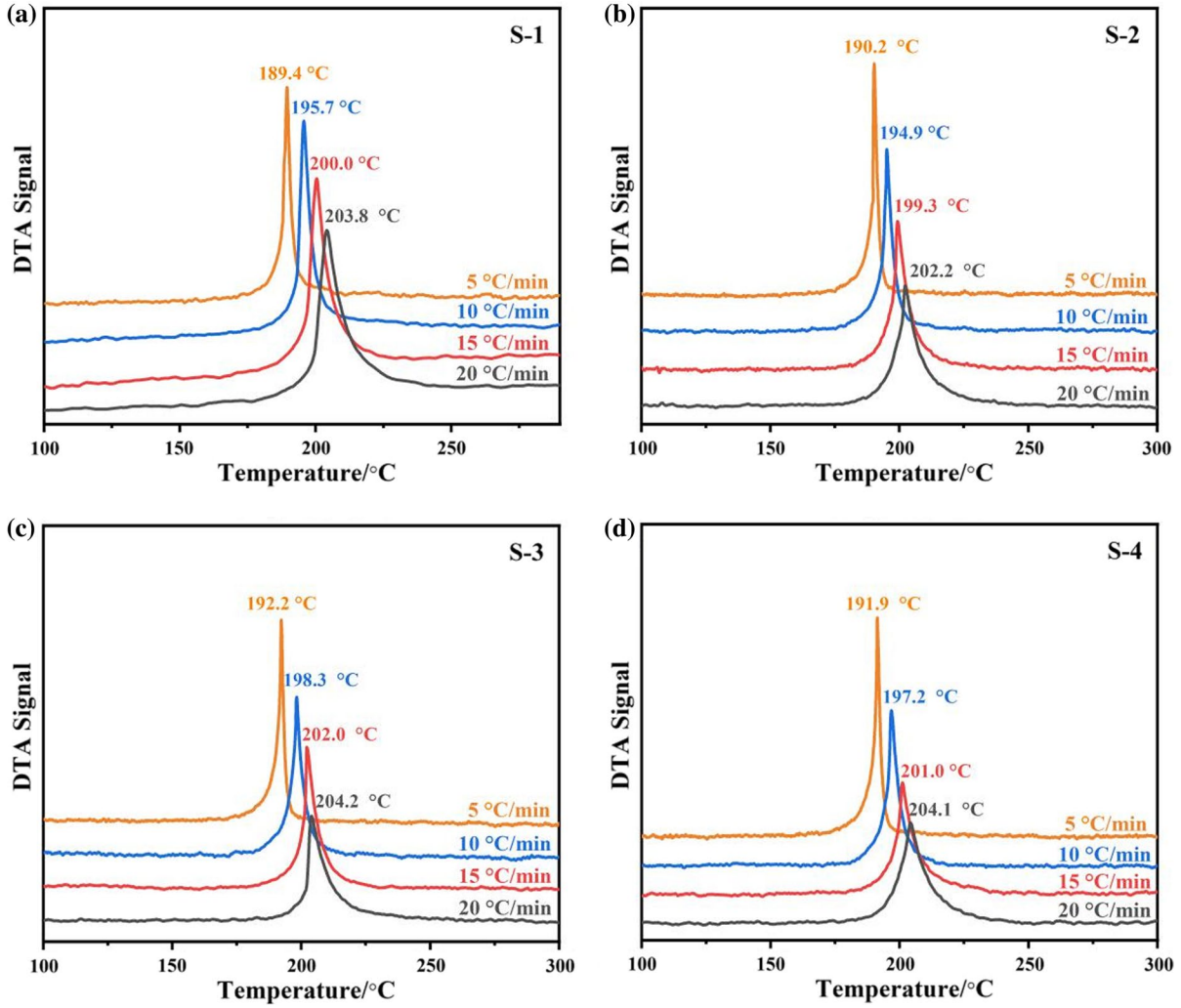

Fig. 6 DTA curves of nitrocellulose sample S-1 (**a**), S-2 (**b**), S-3 (**c**) and S-4 (**d**) at different heating rates

pre-exponential factor; T_{pi} is the peak temperature of the DTA curve at coefficients of β_i, b, c, and d (Table S3); and T_{bp0} is the critical temperature of the thermal explosion. The results obtained using these methods were listed in Table 4 and Table S4.

Compared with nitrocellulose S-1, the T_{p0} of nitrocellulose samples S-2–S-4 increased by 1.5 °C, 3.4 and 4.3 °C, and the T_{bp0} increased by 0.1, 1.8 and 2.8 °C, respectively. In addition, the activation

Table 4 Thermal decomposition parameters of nitrocellulose samples S-1–S-4

Sample	Stabilizer	E_a/kJ·mol^{-1}		log A/s^{-1}		R^2	T_{p0}(°C)	T_{bp0}(°C)
		Value	σ	Value	σ			
S-1	–	170.1	1.06	14.6	2.26	0.9920	179.6	190.0
S-2	**3a**	200.0	1.97	17.9	4.20	0.9863	181.1	190.1
S-3	**3b**	202.9	0.53	18.4	1.12	0.9987	183.0	191.8
S-4	**3c**	204.5	1.24	18.2	2.63	0.9929	183.9	192.8

σ, uncertainties of the computations

energy of S-2–S-4 was significantly lower than that of nitrocellulose S-1.

The process of generating autocatalytic products at a certain temperature is called the thermal history of nitrocellulose. The influence of thermal history on the thermal decomposition of nitrocellulose samples was investigated with the DSC interruption and re-scanning method. The obtained DSC curves were shown in Fig. 7, and the thermal decomposition parameters were shown in Table 5. The release of nitrocellulose thermal decomposition products increased with interrupt temperature, the initial and peak temperatures moved to low temperatures, and the peak width gradually widened. After three times of heating, the peak temperature of the thermal decomposition of nitrocellulose S-1 decreased by 5.1 °C. However, **3a–c** reduced the influence of thermal history on the thermal decomposition of nitrocellulose, and the peak temperatures of S-2, S-3, and S-4 only decreases by 3.4, 3.4 and 3.0 °C after three times of heating.

The linear fitting curves of the peak temperature gradient (γ) of nitrocellulose samples S-1–S-4 at different initial conversion rates (α_0) were shown in Fig. 8. The results showed that the slope and intercept of the fitting curve of S-1 was the largest, indicating that the thermal decomposition of nitrocellulose S-1 was the most seriously affected by the thermal history. These results showed that **3a–c** interacted with the thermal decomposition products

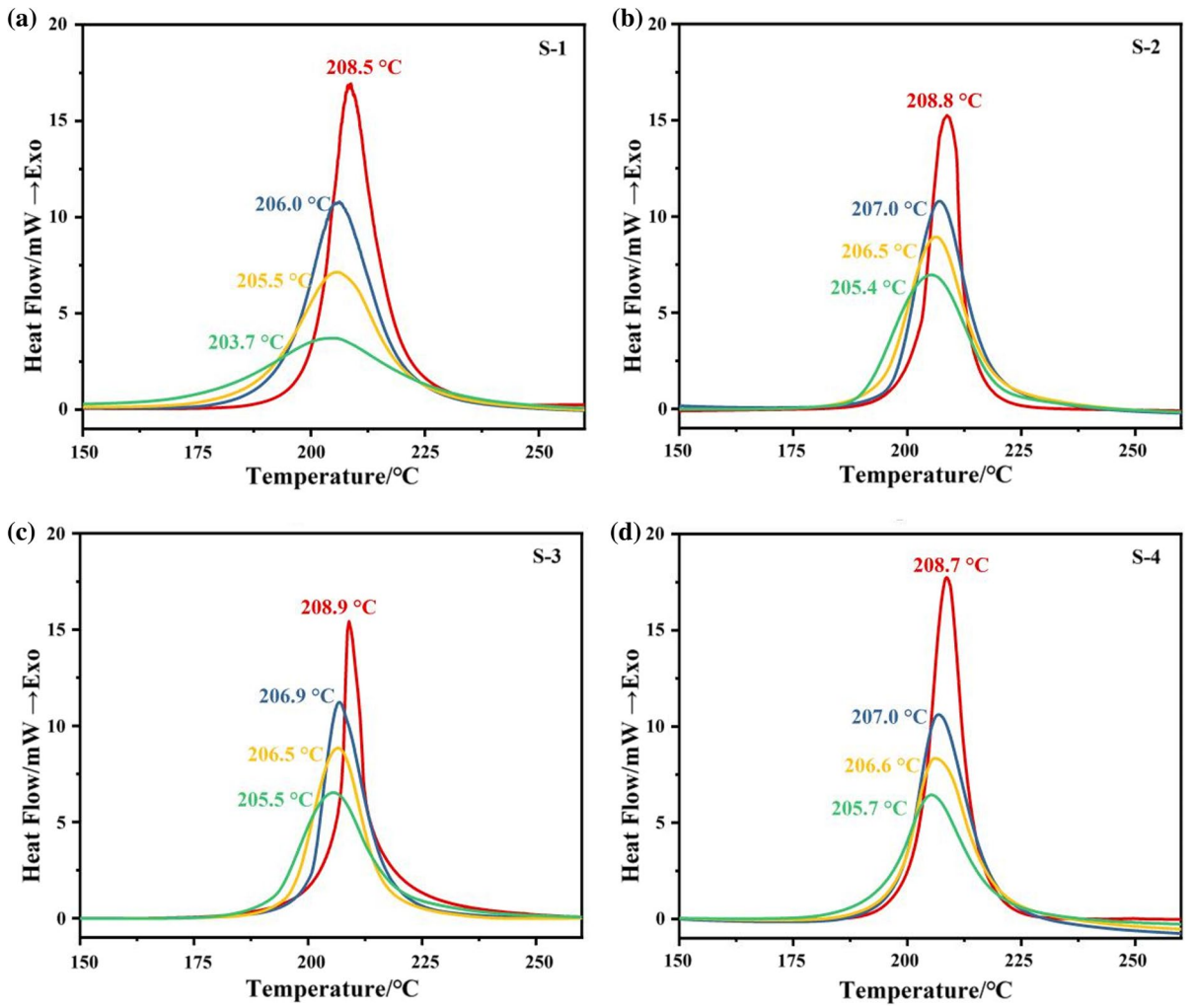

Fig. 7 DSC curves of nitrocellulose sample S-1–S-4 by the interruption and re-scanning method

Table 5 Conditions and results of the DSC tests of the "interruption and re-scanning" method

Sample	Stab	T_{onset}/°C	T_p/°C	ΔH/J·g^{-1}	Sample	Stab	T_{onset}/°C	T_p/°C	ΔH/J·g^{-1}
S1-1#	–	200.5	208.5	2207	S3-1#	**3b**	202.9	208.9	1893
S1-2#	–	194.1	206.0	2151	S3-2#	**3b**	198.6	206.9	1846
S1-3#	–	189.2	205.5	1692	S3-3#	**3b**	196.3	206.5	1257
S1-4#	–	180.9	203.7	941	S3-4#	**3b**	195.7	205.5	975
S2-1#	**3a**	201.8	208.8	1881	S4-1#	**3c**	202.9	208.7	1936
S2-2#	**3a**	198.5	207.0	1846	S4-2#	**3c**	198.5	207.0	1871
S2-3#	**3a**	196.1	206.5	1274	S4-3#	**3c**	196.2	206.6	1431
S2-4#	**3a**	195.0	205.4	998	S4-4#	**3c**	195.3	205.7	1039

of nitrocellulose and inhibited the autocatalytic thermal decomposition of nitrocellulose.

The central region of a large accumulation of nitrocellulose is mostly adiabatic. Therefore, in the evaluation of the thermal stability of the nitrocellulose samples S-1–S-4, thermal decomposition parameters under adiabatic conditions should be considered. The thermal decomposition parameters of samples under adiabatic conditions can be measured through ARC method. The adiabatic decomposition curves of S-1–S-4 with an initial temperature of 100 °C were shown in Fig. 9. After 9, 11, 11, and 12 heating procedures, the nitrocellulose samples were self-exothermic. The initial temperature of the exothermic reaction of nitrocellulose was increased by **3a–c**. In addition, the heat rate-temperature curves of S-1–S-4 were shown in Fig. S19.

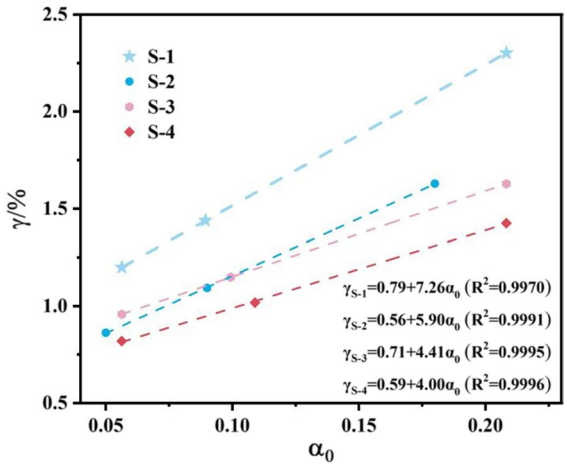

Fig. 8 Relation curve between γ and α_0 of nitrocellulose samples S-1–S-4

The experimental conditions of nitrocellulose at the self-accelerating decomposition stage were shown in Table 6. The maximum temperature rise rate of S-1 was 1.08 °C min^{-1}, whereas the rates of S-2, S-3, and S-4 were 0.30, 0.82, 0.74, and 0.59 °C min^{-1}. The results showed that **3a–c** can increase the initial decomposition temperature and decomposition pressure of nitrocellulose.

Sample S-1–S-4 were graded with the reaction risk assessment method, and the thermal reaction risk was divided into four grades: I, II, III, and IV (Saraf et al. 2003), the reaction risk decreased gradually with increasing grade. The hazard classification for nitrocellulose samples S-1–S-4 were shown in Fig. 10. The results showed that **3a–c** can effectively reduce the thermal risk of nitrocellulose, the initial decomposition temperature of nitrocellulose gradually increased, and the amount of heat released gradually decreased.

Stabilization mechanism

The NO· scavenging capacities of **3a–c** were measured through ESR, and the results were shown in Figs. 11(a–c). After the addition of **3a–c**, the signal of NO· was weakened, and the signal of NO· decreased with increasing **3a–c** concentration, indicating that **3a–c** had excellent scavenging ability for NO·.

The nitrogen oxide radical scavenging rates of **3a–c** were shown in Fig. 11(d). The fitting curves can be expressed as follows:

$$\eta = a \times C^{b}$$

where C denotes the concentrations of **3a–c** and η represents the nitrogen oxide radical scavenging

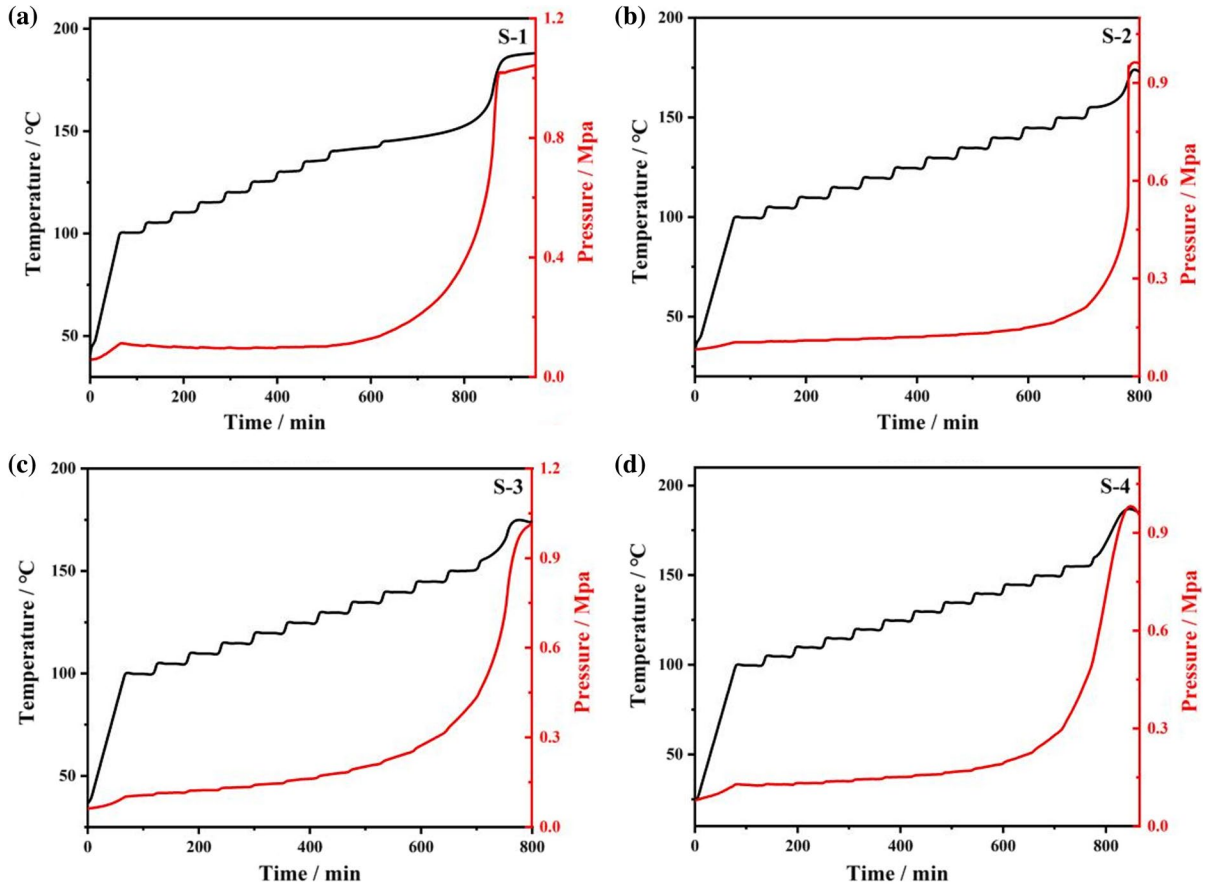

Fig. 9 Adiabatic decomposition curves of nitrocellulose sample S-1–S-4

Table 6 Adiabatic decomposition parameters of S-1–S-4

Sample	S-1	S-2	S-3	S-4
Stabilizer	–	**3a**	**3b**	**3c**
T_o/°C	146.12	160.91	163.54	161.92
P_o/MPa	0.181	0.367	0.516	0.444
m_o/°C min^{-1}	0.030	0.342	0.437	0.330
T_f/°C	188.04	174.05	174.76	176.97
P_f/MPa	1.039	0.965	1.013	0.979
m_m/°C min^{-1}	1.08	0.82	0.74	0.59
T_m/°C	172.08	168.27	167.92	175.17
ΔT_{ad}/°C	41.93	13.14	11.22	15.05

T_o Initial decomposition temperature; P_o Initial decomposition pressure; m_o Initial temperature rise rate; T_f Maximum decomposition temperature; P_f Final pressure; m_m Maximum temperature rise rate; T_m Temperature at maximum temperature rise rate; ΔT_{ad} Adiabatic temperature rise

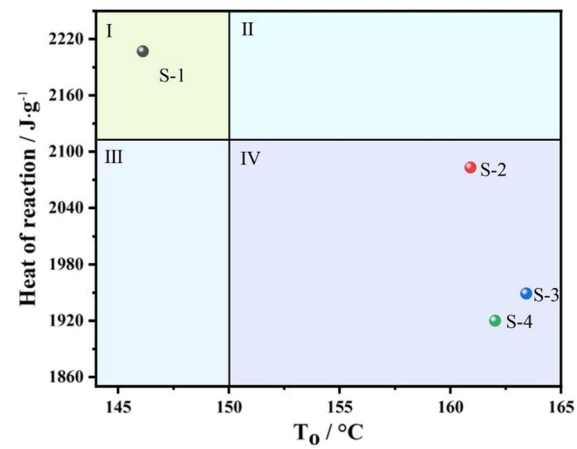

Fig. 10 Hazard classification for nitrocellulose samples S-1–S-4

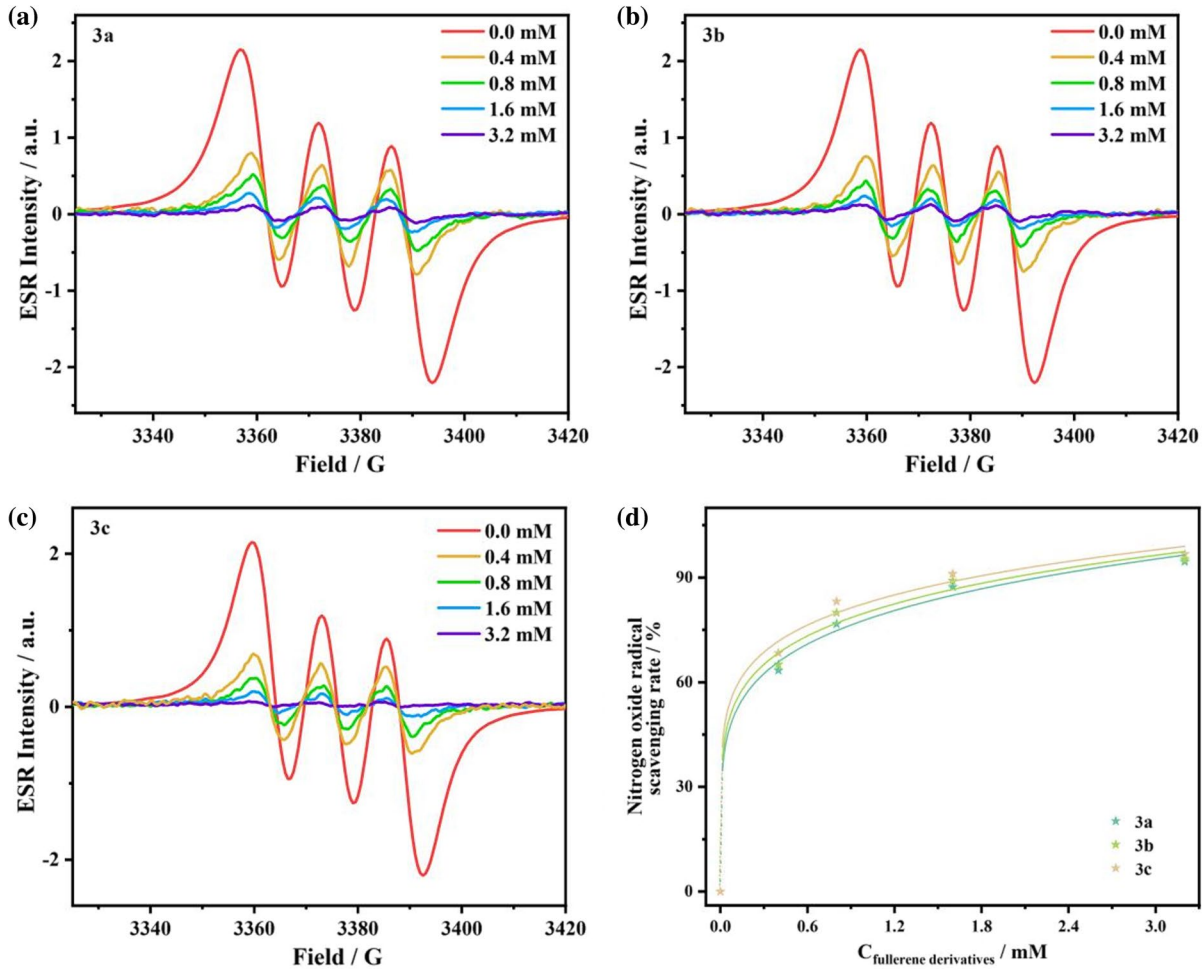

Fig. 11 ESR curves of nitrogen oxide radical scavenging of **3a–c** with different concentrations (**a**–**c**) and nitrogen oxide radical scavenging rates (**d**)

Table 7 Fitting parameters of **3a–c**

Stabilizer	3a	3b	3c
a	77.8989	79.9242	82.6533
b	0.1836	0.1704	0.1546
R^2	0.9489	0.9114	0.9047

Table 8 Nitrogen oxide radical scavenging activity of **3a–c**

Stabilizer	3a	3b	3c
IC50 (mM)	0.247	0.215	0.211
95% CI (mM)	0.123–0.358	0.092–0.315	0.069–0.301

rates. The corresponding parameters were shown in Table 7.

The values of 50% inhibitory concentration (IC50) and 95% confidence interval (CI) of **3a–c** were shown in Table 8, and only 0.247, 0.215 and 0.211 mM of **3a–c** can achieve the semi-inhibition of nitrogen oxide free radical. The results showed that **3a–c** have an extremely high scavenging effect on NO· radical, and only a small amount of **3a–c** can satisfy the 50% inhibitory of the NO· radical.

The infrared spectra of the secondary derivatives of **3a–c** reaction with NO_x were shown in Fig. 12, which was extracted by CS_2. The NO_2 group was obvious in the infrared spectra of the intermediate

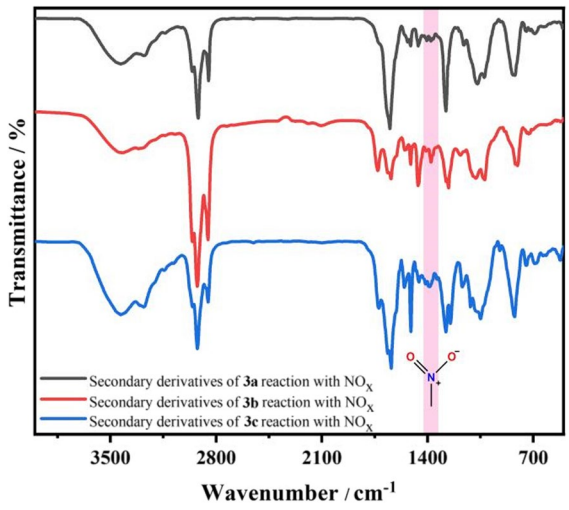

Fig. 12 FT-IR spectra of **3a–c** and intermediate with nitrogen oxides

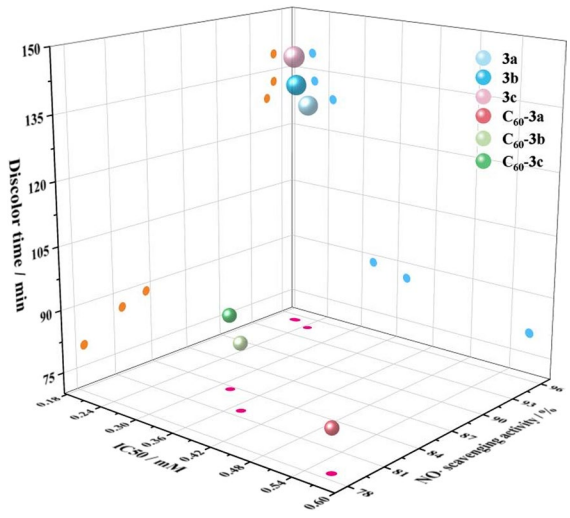

Fig. 13 Comparison of thermal stability of fullerene-based stabilizer with different number of carbon atoms

after the reaction of **3a–c** with nitrocellulose. The results showed that **3a–c** can react with the nitrogen oxides generated by the thermal decomposition of nitrocellulose, and finally form nitro-substituted fullerene derivatives.

Finally, the thermal stability of nitrocellulose samples is affected not only by the functional groups but also by the number of carbon atoms in fullerenes. Based on previously reported data (Li et al. 2020), the thermal stability of the fullerene-based stabilizers with different fullerene was compared. Discoloration time in methyl violet paper, semi-inhibitory concentration (IC50) of NO· and the NO· scavenging rate at 1.2 mM stabilizer concentration were showed in Fig. 13 and Table S5. The results showed that the higher the number of carbon atoms of fullerenes, the better the thermal stability of the fullerene-based stabilizer on nitrocellulose and the scavenging activity of nitrogen oxide radicals. In addition, we compared the stability of typical traditional stabilizer (DPA) with that of fullerene-based stabilizer, and the results were showed in Table S5. The results showed that the unique stabilization mechanism of fullerene-based stabilizers make its stability to nitrocellulose significantly higher than that of DPA.

Conclusion

A serious of arylmalonamide[70]fullerocyclopropanes (**3a–c**) were synthesized by Prato reaction and their structures were characterized with FT-IR, UV–Vis, LC–MS, and NMR. The reaction has the advantages of convenient raw material, mild reaction conditions, high product yield, and easy amplification, providing a means for the subsequent large-scale synthesis of [70]fullerene-based stabilizers. Isothermal thermal analysis confirmed the superior thermal stability of **3a–c** to nitrocellulose even at high temperature, the safe storage life of nitrocellulose at 50 °C can be increased by 31.94 years at most. Non-isothermal thermal analysis showed that the critical temperature of thermal explosion of nitrocellulose could be increased by 2.8 by **3a–c**. At the initial stage of the thermal decomposition of nitrocellulose, **3a–c** can react with nitrogen oxides and other autocatalytic products, thus inhibiting the autocatalytic thermal decomposition of nitrocellulose. In addition, **3a–c** maintains good thermal stability under adiabatic conditions. This finding is of great significance to the safe storage of nitrocellulose under practical conditions. This work provides a novel idea for the design and large-scale preparation of [70]fullerene-based stabilizers.

Acknowledgments This work was supported by the financial support received from National Natural Science Foundation of China (51972278), Associated Foundation of Xi'an Modern

Chemistry Research Institute (No. 204-J-2020-2634), and Open Project of State Key Laboratory of Environment-friendly Energy Materials (Southwest University of Science and Technology, No. 21fksy19).

Declarations

Conflict of interest The authors declare that they have no conflict of interest.

References

Agrawal JP, Surve RN, Mehilal M, Sonawane SH (2000) Some aromatic nitrate esters: synthesis, structural aspects, thermal and explosive properties. J Hazard Mater 77:11–31

Butts CP, Jazdzyk M (2003) The preparation and structures of non-hydrocarbon functionalised fullerene-diamine adducts. Chem Commun 34:1530–1531

Chai ZH, Luo LQ, Jin B, Zhao Y, Xiao LPC, Li G, Zhang QC, Peng RF (2020) Fullerene stabilizer 4,11,15,30-tetraarylamino fullerenoarylaziridine: regioselective synthesis, crystallographic characterization derivatives, and potential application as propellant stabilizer. ACS Appl Energy Mater 3:3005–3014

Cherif MF, Trache D, Benaliouche F, Chelouche S, Tarchoun AF, Mezroua A (2020a) Effect of Kraft lignins on the stability and thermal decomposition kinetics of nitrocellulose. Thermochim Acta 692:178732

Cherif MF, Trache D, Benaliouche F, Chelouche S, Tarchoun AF, Chelouche S, Mezroua A (2020b) Organosolv lignins as new stabilizers for cellulose nitrate: thermal behavior and stability assessment. Int J Biol Macromol 164:794–807

Cherif MF, Trache D, Benaliouche F, Chelouche S, Tarchoun AF, Kesraoui M, Abdelaziz A (2021) Mordenite zeolite for scavenging nitroxide radicals and its effect on the thermal decomposition of nitrocellulose. J Energ Mater. https://doi.org/10.1080/07370652.2021.1998250

De Klerk WPC (2015) Assessment of stability of propellants and safe lifetimes. Propell Explos Pyrot 40(3):388–393

Dennler G, Scharber MC, Brabec CJ (2009) Polymer-fullerene bulk-heterojunction solar cells. Adv Mater 21(13):1323–1338

Dogru M, Handloser M, Auras F, Kunz T, Medina D, Hartschuh A, Knochel P, Bein T (2012) A photoconductive thienothiophene-based covalent organic framework showing charge transfer towards included fullerene. Angew Chem Int Edit 52:2920–2924

Dresselhaus MS, Dresselhaus G, Eklund PC (1996) Science of fullerenes and carbon nanotubes. Academic Press, Cambridge, pp 437–438

Drzyzga O (2003) Diphenylamine and derivatives in the environment: a review. Chemosphere 53(8):809–818

Fryš O, Bajerová P, Eisner A, Skládal J, Ventura K (2011) Utilization of new non-toxic substances as stabilizers for nitrocellulose-based propellants. Propell Explos Pyrot 36(4):347–355

Hassan MA (2001) Effect of malonyl malonanilide dimmers on the thermal stability of nitrocellulose. J Hazard Mater 88(1):33–49

Jia G, Wang HF, Yan L, Wang X, Pei RJ, Yan T, Zhao YL, Guo XB (2005) Cyto-toxicity of carbon nanomaterials: single-wall nanotube, multi-wall nanotube, and fullerene. Environ Sci and Technol 39(5):1378–1383

Katoh K, Yoshino S, Kubota S, Wada Y, Ogata Y, Nakahama M, Kawaguchi S, Arai M (2007) The effects of conventional stabilizers and phenol compounds used as antioxidants on the stabilization of nitrocellulose. Propell Explos Pyrot 32(4):314–321

Krishna V, Stevens N, Koopman B, Moudgil B (2010) Optical heating and rapid transformation of functionalized fullerenes. Nature Nanotechnol 5(5):330–334

Krumlinde P, Ek S, Tunestål E, Hafstrand A (2016) Synthesis and characterization of novel stabilizers for nitrocellulose-based propellants. Propell Explos Pyrot 42(1):78–83

Li G, Jin B, Chai ZH, Liao L, Chu SJ, Peng RF (2020) Synthesis and stabilization mechanism of novel stabilizers for fullerene-malonamide derivatives in nitrocellulose-based propellants. Polym Test 86:106493

Liao L, Jin B, Guo ZC, Xian F, Hou CJ, Peng RF (2021) Fullerene bisadduct stabilizers: the effect of different addition positions on inhibiting the autocatalytic decomposition of nitrocellulose absorbed nitroglycerin. Def Tech 17(6):1944–1953

Lindblom T (2002) Reactions in stabilizer and between stabilizer and nitrocellulose in propellants. Propell Explos Pyrot 27(4):197–208

Luo LQ, Jin B, Xiao YY, Zhang QC, Chai ZH, Huang Q, Chu SJ, Peng RF (2019) Study on the isothermal decomposition kinetics and mechanism of nitrocellulose. Polym Test 75:337–343

Lussier LS, Bergeron E, Gagnon H (2006) Study of the daughter products of Akardite-II. Propell Explos Pyrot 31(4):253–262

Markovic Z, Trajkovic V (2008) Biomedical potential of the reactive oxygen species generation and quenching by fullerenes. Biomater 29:3561–3573

Naud DL, Brower KR (1992) Pressure effects on the thermal decomposition of nitramines, nitrosamines, and nitrate esters. J Org Chem 57:3303–3308

Saraf SR, Rogers WJ, Mannan WS (2003) Using screening test data to recognize reactive chemical hazards. J Hazard Mater 104:255–267

Shehata AB, Hassan MA, Nour MA (2003) Effect of new poly 2-acryloyl-N, N'-bis (4-nitrophenyl) propandiamide and poly 2-acryloyl-N, N'-bis (4-methylphenyl) propandiamide and their synergistic action on the stability of nitrocellulose. J Hazard Mater 102(2/3):121–136

Srinivas D, Ghule VD (2016) Synthesis of nitrate ester and nitramine derivatives of polyfluoro alkyl compounds for high energy materials. RSC Adv 6(10):7712–7716

Sun ZD, Fu XL, Yu HJ, Fan XZ, Ju XH (2017) Theoretical study on stabilization mechanisms of nitrate esters using aromatic amines as stabilizers. J Hazard Mater 339:401–408

Tang QF, Fan XZ, Li JZ, Bi FQ, Fu XL, Zhai LJ (2017) Experimental and theoretical studies on stability of new

stabilizers for *N*-methyl-*P*-nitroaniline derivative in CMDB propellants. J Hazard Mater 327:187–196

Tarchoun AF, Trache D, Krumm B, Derradji M, Bessa W (2021) Design and characterization of new advanced energetic biopolymers based on surface functionalized cellulosic materials. Cellulose 28:6107–6123

Tarchoun AF, Trache D, Klapötke TM, Abdelaziz A, Bekhouche S, Boukeciat H, Sahnoun N (2022a) Making progress towards promising energetic cellulosic microcrystals developed from alternative lignocellulosic biomasses. J Energ Mater. https://doi.org/10.1080/07370652.2022.2032484

Tarchoun AF, Trache D, Klapötke TM, Slimani K, Abdelaziz BB, A, Bekhouche S, Bessa W, (2022b) Valorization of esparto grass cellulosic derivatives for the development of promising energetic azidodeoxy biopolymers: synthesis, characterization and isoconversional thermal kinetic analysis. Propell Explos Pyrot 47(3):e202100293

Tarchoun AF, Sayah ZBD, Trache D, Klapötke TM, Belmerabt M, Abdelaziz A, Bekhouche S (2022c) Towards investigating the characteristics and thermal kinetic behavior of emergent nanostructured nitrocellulose prepared using various sulfonitric media. J Nanostruct Chem. https://doi.org/10.1007/s40097-021-00466-x

Tong Y, Wu ZP, Yang C, Yu J, Zhang X, Yang S, Deng X, Xu Y, Wen Y (2001) Determination of diphenylamine stabilizer and its nitrated derivatives in smokeless gunpowder using a tandem MS method. Analyst 126(4):480–484

Trache D, Khimeche K (2013) Study on the influence of ageing on chemical and mechanical properties of N, N'-dimethyl-N, N'-diphenylcarbamide stabilized propellants. J Therm Anal Calorim 111:305–312

Trache D, Tarchoun AF (2019) Analytical methods for stability assessment of nitrate esters-based propellants. Crit Rev Anal Chem 49:415–438

Wang GW, Yang HT, Wu P, Wang CZ (2010) Reaction of [70] Fullerene with tetraethyl methylenediphosphonate or diethyl (cyanomethyl)phosphonate revisited. Eur J Org Chem 29:5714–5721

Wang K, Liu DB, Xu S, Cai GW (2015) Research on the thermal history's influence on the thermal stability of EHN and NC. Thermochim Acta 610:23–28

Wang B, Xin L, Wang Z, Deluca LT, Liu Z, You F (2017) Preparation and properties of a *n*RDX-based propellant. Propell Explos Pyrot 42:649–658

Xie QS, Eduardo PC, Luis E (1992) Electrochemical detection of C_{60}^{6-} and C_{70}^{6-}: enhanced stability of fullerides in solution. J Am Chem Soc 114(10):3978–3980

Zayed MA, Soliman AAW, Hassan MA (2000) Evaluation of malonanilides as new stabilizers for doubleBase propellants(I). J Hazard Mater 73(3):237–244

Zayed MA, Mohamed AA, Hassan MAM (2010) Stability studies of double-base propellants with centralite and malonanilide stabilizers using MO calculations in comparison to thermal studies. J Hazard Mater 179(1–3):453–461

Zhao Y, Jin B, Peng RF, Ding L, Zheng T (2020a) Novel fullerene-based stabilizer for scavenging nitroxide radicals and its behavior during thermal decomposition of nitrocellulose. J Hazard Mater 191:121857–121863

Zhao Y, Jin B, Peng RF, Zheng T (2020b) Interaction of nitrocellulose with pentaacyloxyphenyl fullerene derivatives: autocatalytic inhibition in thermal decomposition of nitrocellulose. Cellulose 27:3611–3622